IOSR Journal of Mechanical and Civil Engineering (IOSR-JMCE)
e-ISSN: 2278-1684,p-ISSN: 2320-334X, Volume 17, Issue 6 Ser. II (Nov. – Dec. 2020), PP 22-37
www.iosrjournals.org

Numerical Investigation of Non-Newtonian Nanofluid Flow in Spiral Pipe

Amir haghighatkhah *, Milad abdollahikahriz.
1. Master of Mechanical Engineering,
Doctor of Mechanical Engineering,

Abstract
Fluids can be classified from different perspectives. From the perspective of fluid behavior under the influence of shear stress, the fluids can be classified into Newtonian and non-Newtonian fluids. Newtonian fluid is a material in which shear stress without yield stress (at zero shear rate is zero shear stress) is only a linear function of shear rate and in this material shear stress to shear rate is called viscosity. In non-Newtonian fluids one of the two Newtonian fluid conditions (zero yield stress condition or shear stress linearity condition in terms of shear rate) or both conditions are not met simultaneously. In other words, it can be said that a non-Newtonian fluid is a fluid in which either the shear stress diagram is nonlinear in shear rate or if the diagram is linear it does not cross the origin of the coordinates.
In this study, non-Newtonian fluid flow in spiral tubes with different cross-sections is investigated. Three circular, oval and square cross sections are provided for the spiral tube and the fluid flow is investigated in steady and three-dimensional state. For numerical simulation, the commercial software Ennis Fluent, which is a subset of Ennis software, is used specifically to simulate fluid flows. For different Reynolds numbers, different cross-sectional area of pipe and different torsion steps, mean Nusselt number, local Nusselt number, vorticity, friction coefficient and pressure drop have been measured and the influence of the mentioned parameters on each of the variables has been investigated. . It is shown that the spiral tube with a square cross-section generally exhibits the best thermal performance, followed by a spiral tube with an elliptical cross-section. In general, the spiral tube with a circular cross-section shows the weakest thermal performance among the three cross-sections examined. This equation can be found in the hydraulic diameter of the cross-section so that the hydraulic diameter of the square cross-section is obtained by 4, while the hydraulic diameter of the circular cross-section is 2. Thus the hydraulic diameter of the square cross-section is approximately twice that of the circular cross-section. For example, for a spiral tube with a circular cross-section and a volume fraction of 4% the average Nusselt number is approximately equal to the average Nusselt number for a spiral tube with a square cross-section and a volume fraction of 4% and an input rate of 0.5 m / s.

Keywords: *Spiral pipe, Non-Newtonian fluid, Numerical simulation, Fluent software.*

Date of Submission: 16-11-2020 Date of Acceptance: 02-12-2020

I. Introduction

Non-Newtonian fluid mechanics has been the subject of much interest by researchers since the late 19th century. And in those years the basic theories of this science were built. Among non-Newtonian fluids, viscoelastic fluids have received much attention due to their many applications and have been the subject of much research. Non-Newtonian fluids are widely used in military, medical, and industrial activities, which have long been the focus of attention. The science of studying non-Newtonian fluid flow has become known as rheology today, and because of the specific properties of such fluids, different and unexpected behaviors of such fluids occur. The purpose of this study was to investigate the non-Newtonian fluid flow with power model and its heat transfer in spiral tubes with different cross sections, mathematical modeling, its solution and then analyzing and evaluating the existing solution.

Fluid flow in spiral tubes is of particular importance. These tubes are used in heat exchangers and condensers and coils. These pipes have a relatively simple geometry and a relatively complex flow shape.

There have been many studies on heat transfer in spiral tubes. The increase in flow pressure drop in curved tubes was first reported by Grindley and Gibson [1] compared to conventional pipe pressure drop. Hawthorne[2] was the first researcher to propose a numerical method for fully developed flow in curved tubes. Itō [3] provided a relation for the coefficient of friction in terms of Reynolds number and coil curvature ratio. Rogers and Mayhew [4] experimentally studied the experimental heat transfer coefficient and the vapor pressure drop. They proposed relationships for the Nusselt number and the coefficient of friction in terms of Reynolds

number, coil curvature ratio and Prantel number for turbulent intra-coil flow. Austin and Seader [5] experimentally examined the velocity profile in the inlet area of the pipe. They stated that as the number of religions increased, the length of the redevelopment area would also increase.

Until now, various studies have been conducted on combined heat transfer and fluid to fluid heat transfer in heat exchangers. This may include experimental research on the natural displacement heat transfer of a helical coil by Ali et al. [6] who investigated free displacement heat transfer for turbulent flow. They performed experiments on coils with 4 different curvature ratios and rounds of 5 and 10 and, using the results, obtained the relation of heat transfer coefficient in Rayleigh number. Moulin et al. [7] conducted an experimental and numerical study on flow in curved tubes and stated that secondary flow had no significant effect on Reynolds numbers below 20. Bhattacharya et al. [8] determined the optimal degree of curvature in a fully developed slow flow with forced displacement in the coil. Chen et al [9] investigated the combined effects of rotation and curvature on flow pattern, pressure drop, temperature distribution, and Nusselt number of spiral tubes. Ko [10] obtained the Reynolds number and the optimal curvature by analyzing the flow and heat transfer in a coil having a constant flux. Kurnia et al[11] simulated the spiral tubes with non-circular cross-sections numerically and showed that the heat transfer coefficient in these channels was higher than that of direct channels. In another study, the same people investigated the performance of heat transfer in cooling channels with different designs [12]. In 2011, Sasmito et al. [13] investigated the heat transfer of aluminum-oxide water and copper-oxide nano-fluids for simple, conical, planar, and spiral square tubes. And it was found that adding one percent volumetric concentration of nanoparticles improved the heat transfer performance but did not recommend values above 1 percent and also found that flat spiral tubes performed better. In addition, the performance of aluminum nano-fluid is better than that of copper-nano-fluid. In their study, the channels were parallel, wavy, zigzag, with diagonal fin and spiral tubes, and their results showed that the spiral tube had a higher heat transfer coefficient than other types. Mirgolbabaeiet al. [14] performed a numerical study on the heat transfer of a helical coil with a cylindrical shell at different Reynolds and Riley numbers, as well as different tube-to-coil diameter and dimensional ratio. Their difference with similar work was to consider boundary conditions for a fluid-to-fluid heat exchanger rather than constant wall temperature and heat flux conditions.

Jundika et al. [15] demonstrated that non-Newtonian carboxymethyl cellulose CMC solutions increase the heat transfer performance (twice) compared to water. However, the pressure needs to be increased up to four times higher. It was also found that the heat transfer function and pressure drop were not linear with the CMC concentration. The vertical coil provides the best heat transfer performance over the flat coil and cone coil, but due to its high pressure drop, use must be careful.

Jia-dong et al. [16] reported that in flat spiral tubes with an elliptical cross-section, the heat transfer coefficient and Nusselt number increase with increasing water mass flow or increasing rotational step. The maximum heat transfer coefficient and the maximum Nusselt number are obtained when the radius ratio is equal to one. In addition, the liquid particles spiral along the pipe and its velocity changes periodically. The particle flow and the spiral motion frequency are significantly reduced with increasing radius ratio. Wang et al. [17] studied spiral corrugated tubes. They obtained optimal values for Reynolds, Nusselt and wave-to-diameter ratios and wave valley-to-diameter ratios. Liu et al. [18] investigated the heat transfer of carbon dioxide in supercritical conditions in spiral tubes. A similar study by Houjian, Xiaowei Li et al [19] on supercritical water flow has also been conducted.

II. The governing equations

In this study, a single-phase model is used to investigate the heat transfer of non-Newtonian nanofluid flow in the helical channel. For this purpose, the governing equations including the equation of continuity, momentum and energy must be solved for the flow field. To solve these equations, the numerical method and, in particular, the commercial software Ennis Fluent, which is a finite volume software, is used. Since the surface of the helical channel is considered as circular and non-circular once, the governing equations are introduced in the two cylindrical and Cartesian coordinate systems. First, the rejection equations of the cylindrical coordinate system are discussed.

Dimensional governing equations including mass, momentum and energy survival equations for the cylindrical coordinate system are written as follows:

$$\frac{\partial u}{\partial x}+\frac{1}{r}\frac{\partial}{\partial r}(rv)=0 \quad (1)$$

$$\rho\left(u\frac{\partial u}{\partial x}+v\frac{\partial u}{\partial r}\right)=-\frac{\partial P}{\partial x}+\left(\frac{\partial \tau_{xx}^{T}}{\partial x}+\frac{1}{r}\frac{\partial}{\partial r}(r\tau_{rx}^{T})\right) \quad (2)$$

$$\rho\left(u\frac{\partial v}{\partial x}+v\frac{\partial v}{\partial r}\right)=-\frac{\partial P}{\partial r}+\left(\frac{\partial \tau_{xr}^{T}}{\partial x}+\frac{1}{r}\frac{\partial}{\partial r}(r\tau_{rr}^{T})-\frac{\tau_{\theta\theta}^{T}}{r}\right) \quad (3)$$

$$\rho cu\frac{\partial T}{\partial x}+\rho cv\frac{\partial T}{\partial r}=\frac{1}{r}\frac{\partial}{\partial r}\left(kr\frac{\partial T}{\partial r}\right)+\frac{\partial}{\partial x}\left(k\frac{\partial T}{\partial x}\right)+\tau_{rx}\left(\frac{\partial u}{\partial r}+\frac{\partial v}{\partial x}\right) \quad (4)$$

By defining the following dimensionless parameters, the following equations can be overwritten as follows:

$X = \frac{x}{D_h}, R = \frac{r}{D_h}, U = \frac{u}{u_{in}}, \theta = \frac{T-T_{in}}{\Delta T}, \Delta T = \frac{q^{"}D_h}{k_f}, P = \frac{\rho}{\rho_{nf}u^2}, L_1 = \frac{L}{D}$(5)

In the above relationships,ρ is density, P is pressure, τ is stress, T is temperature, k is thermal conductivity, D_h is hydraulic diameter, $q^{"}$ is heat flux and L is channel length.

Thus the dimensional equations are written as follows:

$\frac{\partial U}{\partial X} + \frac{\partial V}{\partial R} = 0$(6)

$U\frac{\partial U}{\partial X} + V\frac{\partial U}{\partial R} = -\frac{\partial P}{\partial X} + \frac{1}{Re_{nf}}\left(\frac{\partial}{\partial X}\left(\frac{\partial U}{\partial X}\right)^n + \frac{\partial}{\partial R}\left(\frac{\partial U}{\partial R}\right)\right)^n$ (7)

$U\frac{\partial U}{\partial X} + V\frac{\partial V}{\partial R} = -\frac{\partial P}{\partial X} + \frac{1}{Re_{nf}}\left(\frac{\partial}{\partial X}\left(\frac{\partial V}{\partial X}\right)^n + \frac{1}{R}\times\frac{\partial}{\partial R}R\left(\frac{\partial V}{\partial R}\right)\right)^n - \frac{V^2}{R}$(8)

$U\frac{\partial \theta}{\partial X} + V\frac{\partial \theta}{\partial R} = \frac{1}{Pr_{nf}Re_{nf}}\left(\frac{\partial}{\partial X}\left(\frac{\partial \theta}{\partial X}\right)^n + \frac{1}{R}\times\frac{\partial}{\partial R}R\left(\frac{\partial \theta}{\partial R}\right)\right)^n$ (9)

If the power-law model is used to model non-Newtonian fluid flow, the shear stress (τ) is calculated as follows: [21]:

$\tau = K|\dot{\gamma}|^n \rightarrow |\dot{\gamma}| = 2\left[\left(\frac{\partial v}{\partial r}\right)^2 + \left(\frac{v}{r}\right)^2 + \left(\frac{\partial u}{\partial x}\right)^2\right] + \left[\frac{\partial v}{\partial x} + \frac{\partial u}{\partial r}\right]^2$ *(10)*

In the above relation τ denotes shear stress, K denotes consistency index, $\dot{\gamma}$ denotes shear rate and n denotes power index for power model. The following equation can be used to define the Reynolds number for non-Newtonian fluid [22]. It should be noted that the constant coefficient and power law index as well as the fluid velocity at the inlet of the pipe are essential to calculate the Reynolds number.

$Re = \frac{\rho U^{2-n}D^n}{K}$(11)

The Peclet number and Prandtl number for non-Newtonian fluid are defined as follows: [23]:

$\mathrm{Pr} = \frac{Cp_{nf}.r}{k_{nf}}\left(\frac{\vartheta_{nf}}{D_h}\right)^{n-1}$(12)

In the above relation, ϑ expresses kinematic viscosity.

$Pe = Re.\mathrm{Pr} = \frac{\rho_{nf}.Cp_{nf}.\vartheta_{nf}.D_h}{k_{nf}}$(13)

The governing equations in the Cartesian coordinate system are written as follows:

The continuity equation is written as follows:

$\frac{\partial u}{\partial x} + \frac{\partial v}{\partial y} + \frac{\partial w}{\partial z} = 0$(14)

The momentum equation in the x direction is written as follows:

$u\frac{\partial u}{\partial x} + v\frac{\partial u}{\partial y} + w\frac{\partial u}{\partial z} = -\frac{\partial P}{\partial x} + \frac{1}{Re}\left[\frac{\partial C}{\partial x} + \frac{\partial D}{\partial y} + \frac{\partial E}{\partial z}\right]$(15)

The momentum equation in the y direction is written as follows:

$u\frac{\partial v}{\partial x} + v\frac{\partial v}{\partial y} + w\frac{\partial v}{\partial z} = -\frac{\partial P}{\partial v} + \frac{1}{Re}\left[\frac{\partial F}{\partial y} + \frac{\partial D}{\partial x} + \frac{\partial G}{\partial z}\right]$(16)

The momentum equation in the z direction is written as follows:

$u\frac{\partial w}{\partial x} + v\frac{\partial w}{\partial y} + w\frac{\partial w}{\partial z} = -\frac{\partial P}{\partial z} + \frac{1}{Re}\left[\frac{\partial E}{\partial x} + \frac{\partial G}{\partial y} + \frac{\partial H}{\partial z}\right]$(17)

In the above relationships C, D, E, F, G and H are defined as follows:

$C = 2\left(\frac{\Pi}{2}\right)^{\frac{n-1}{2}}\frac{\partial u}{\partial x}$(18)

$D = \left(\frac{\Pi}{2}\right)^{\frac{n-1}{2}}\left(\frac{\partial u}{\partial y} + \frac{\partial v}{\partial x}\right)$(19)

$E = \left(\frac{\Pi}{2}\right)^{\frac{n-1}{2}}\left(\frac{\partial u}{\partial z} + \frac{\partial w}{\partial x}\right)$(20)

$F = 2\left(\frac{\Pi}{2}\right)^{\frac{n-1}{2}}\frac{\partial v}{\partial y}$(21)

$G = \left(\frac{\Pi}{2}\right)^{\frac{n-1}{2}}\left(\frac{\partial v}{\partial z} + \frac{\partial w}{\partial y}\right)$(22)

$H = 2\left(\frac{\Pi}{2}\right)^{\frac{n-1}{2}}\frac{\partial w}{\partial z}$(23)

$\frac{\Pi}{2} = 2\left[\left(\frac{\partial u}{\partial x}\right)^2 + \left(\frac{\partial v}{\partial y}\right)^2 + \left(\frac{\partial w}{\partial z}\right)^2\right] + \left(\frac{\partial u}{\partial y} + \frac{\partial v}{\partial x}\right)^2 + \left(\frac{\partial w}{\partial y} + \frac{\partial v}{\partial z}\right)^2 + \left(\frac{\partial u}{\partial z} + \frac{\partial w}{\partial x}\right)^2$(24)

The following equations can be defined by the following dimensionless parameters:

$X = \frac{x}{D_h}, Y = \frac{y}{D_h}, Z = \frac{z}{D_h}$(25)

$U = \frac{u}{V_e},\ V = \frac{v}{V_e}, W = \frac{w}{V_e}$(26)

$P = \frac{P-P_0}{\rho V_e^2}$(27)

$Y^+ = \frac{y}{D_h.Re}$(28)

In this study, the power law model is used to study the fluid rheological behavior. Therefore, in spite of the controversies surrounding the determination of nanofluid viscosity, the k and n indices, which represent the power law index and the coherence index, respectively, are also included in the treatments. It should be noted that the value of k and n for different nano-fluids varies depending on the volume fraction of nano-particles in the base fluid. For example, to calculate the value of k and n in water-oxide-copper nanoparticles with a volume fraction of 0.5% to 1.5% assuming the fluid is non-Newtonian, the graph presented by Hojjat et al. [23] can be used.

In order to access the nanofluid properties, either experimental data need to be used that requires time and cost to conduct material properties testing or the equations suggested by researchers, often based on empirical relationships, can also be used. . The second method will be used in this study. The following equations can be used to calculate the density and specific heat capacity of nanofluids [25,24]:

$\rho_{nf} = (1-\emptyset)\rho_f + \emptyset\rho_s$(29)

$(\rho C_p)_{nf} = (1-\emptyset)(\rho C_p)_f + \emptyset(\rho C_p)_s$(30)

In the above relations, $\emptyset$ the volume fraction of nanoparticles and subscripts f, s, and nf are expressed as fluid, nanoparticles, and nanofluids, respectively. To calculate the thermal conductivity of a nanofluid, the following equation can be used: [25]:

$\frac{k_{nf}}{k_f} = 1 + 64.7\emptyset^{0.7460}\left(\frac{d_f}{d_p}\right)^{0.3690} \times \left(\frac{k_p}{k_f}\right)^{0.7476} Pr^{0.9955} Re^{1.2321}$(29)

In relation (29) the non-dimensional numbers Prandtl and Reynolds are defined as follows:

$Pr = \frac{\mu_f}{\rho_f \alpha_f}$(30)

$Re = \frac{\rho_f V_{Br} d_p}{\mu_f} = \frac{\rho_f k_B T}{3\pi\mu_f^2 \lambda_f}$(31)

In the above equations, α_f denotes the basic fluid thermal distribution.

The dynamic viscosity of the base fluid can also be calculated using the following equation:

$\mu_f = A \times 10^{\frac{B}{(T-c)}}$(32)

In the above relation, the coefficients A, B, and C are constant, which for the water-based fluid are ⇂$2.414 \times 10^{-5}\ Pa.s$ ،$247.8K$ and 140K, respectively.

Also in the above relationship, V_{Br} denotes the flow rate of the nanoparticles, which are defined as follows:

$V_{Br} = \frac{k_B T}{3\pi\mu\, d_p \lambda_f} = \frac{k_B}{3\pi d_p \lambda_f} \frac{T}{A\times 10^{\frac{B}{(T-c)}}}$(33)

In the above relation λ_f denotes molecular mean free path. According to the experimental reports presented [25], the above relationship is valid for nanoparticles with dimensions of 11 nanometers up to 150 mm and temperatures of 1 ° C to 71 ° C. In Equation (33), the effect of motion and diameter of nanoparticles is considered to calculate the thermal conductivity coefficient.

The following equations can be used to calculate the flow parameters and heat transfer of non-Newtonian nano fluid flow.

To calculate the local Nusselt number, we can write [26]:

$Nu(x) = \frac{h(x)\times D_h}{k_f}$(34)

Also, the local displacement heat transfer coefficient is defined as follows: [26]:

$h(x) = \frac{q^{"}}{T_w - T_{in}}$(35)

In the above relation, T_w ،$T_{in} and q^{"}$ represent the local wall temperature, mean fluid inlet temperature, and heat flux, respectively. Using equations (34) and (35) and using dimensionless parameters, Already introduced, it can be written:

$Nu(x) = \frac{1}{\theta_s(X)}$(36)

By integrating the above relation on the wall the mean Nusselt number is calculated as follows:

$Nu_{ave} = \frac{1}{L_1}\int_0^{L_1} Nu(x)dX$(37)

The following equations are used to calculate the average friction coefficient [26,25]:

$f = \frac{2.\Delta P.D_h}{L.\rho.u_{in}}$(38)

The following equations can also be used to calculate the coefficients m and n in the Power Law model for non-Newtonian fluid modeling in addition to using the graphs mentioned above:

$m = 32.1\emptyset^2 - 2.295\emptyset + 0.156$(39)

$n = 15.69\emptyset^2 - 0.618\emptyset + 0.536$(40)

It should be noted that the above relationships are valid only for nanofluids with a volume fraction of 0.5% to 4% at 298 K.

III. Problem assumptions

In the present study, the geometry of the problem is considered as three dimensional and incompressible fluid flow. The range of Reynolds numbers used in the present study for the turbulent flow regime is summarized as follows.

1. The flow is three-dimensional and turbulent.
2. The fluid is non-Newtonian and follows the power model and is incompressible.
3. Thermophysical properties of non-Newtonian nano fluid are assumed to be temperature independent.
4. Reynolds is considered to be within the range of a turbulent flow regime.
5. The effects of gravitational acceleration and volume forces have been avoided.

IV. The geometry of the problem

The geometry of the problem consists of a spiral tube with three circular, oval and square sections. The side length of the channel cross-section is considered to be one centimeter. The schematic view of the pipe being considered in this project can be seen in Figure (1).

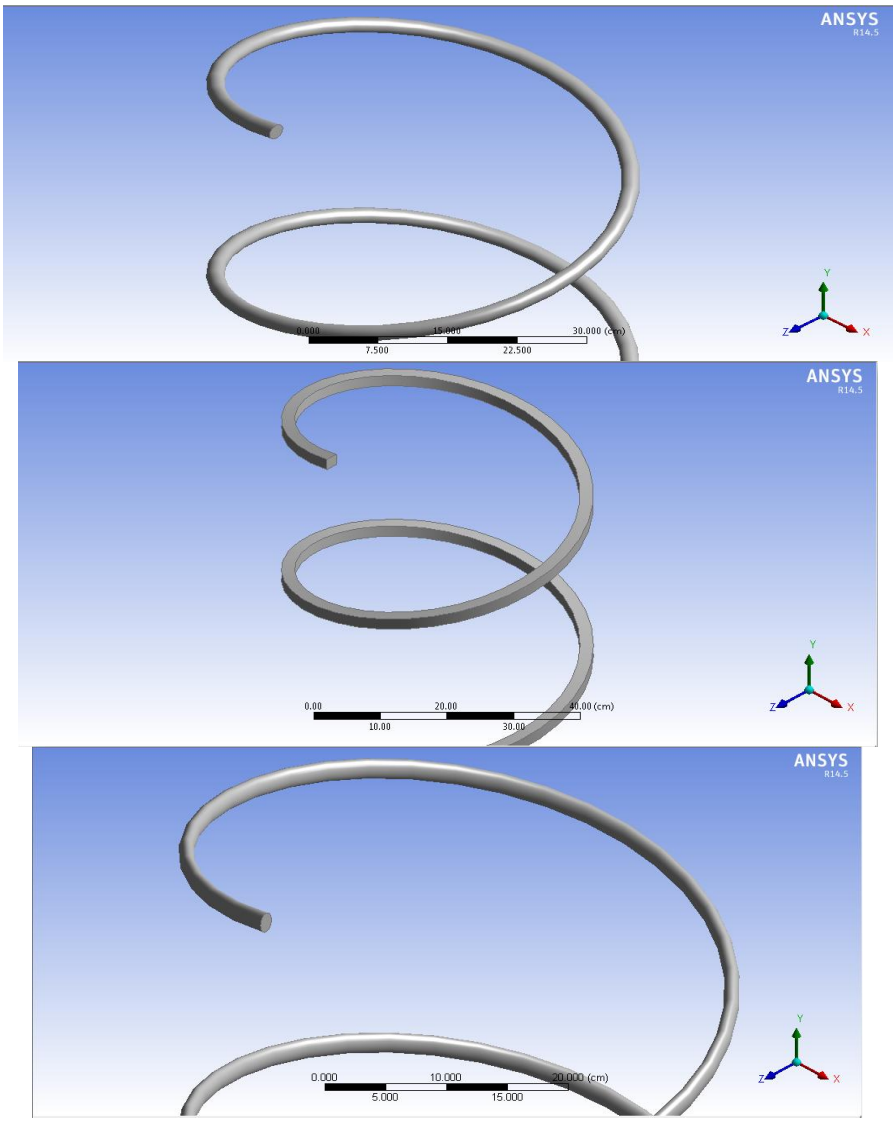

Figure 1. Schematic view of the spiral tube investigated

V. Boundary conditions

The channel input will use the input speed boundary condition. We know that the channel input can be considered as a uniform input speed. At the outlet of the channel, since the fluid is assumed to be discharged into the environment, then the use of the outlet boundary condition is a reasonable and accurate pressure. It should be noted that in this case the output pressure gauge is zero. In the case of canal walls, the term non-slip fluid on the wall should also be used, which assumes that the velocity of the fluid on the wall is equal to the velocity of the wall, and in this case, since the channel wall is constant, it can be said that the fluid velocity on the wall is Channel will be zero.

VI. Calculation of thermodynamic properties of nanofluid

Before calculating the thermophysical properties of water-copper-oxide nanofluids, it is necessary to extract the thermophysical properties of water and copper-oxide nanoparticles alone. These properties are shown in Table (1).

Table 1. Thermophysical properties of water fluid and copper oxide nanoparticles [27]

Thermophysical property	Water	Copper oxide
Density ($\frac{kg}{m^3}$)	998.2	6350
Special heat capacity ($\frac{J}{kg.K}$)	4182	535.6
Thermal conductivity ($\frac{W}{m.K}$)	0.6	69
Viscosity ($\frac{kg}{m.s}$)	0.001003	-

The thermophysical properties of nanofluids are calculated for different volume fractions similar to Table (2).

Table 2. Thermophysical Properties of Water-Oxide Copper Nanofluids for Different Volume Fractions

Volume fraction(%)	Density ($\frac{kg}{m^3}$)	Special heat capacity ($\frac{J}{kg.K}$)	Thermal conductivity ($\frac{W}{m.K}$)	Viscosity ($Pa.s$)	m	n
1	1076.5	3864.2	0.6806	0.000967	0.13626	0.5314
2	1155.8	3592.5	0.7496	0.0011	0.12294	0.5300
3	1235.2	3355.8	0.8199	0.0012	0.11604	0.5318
4	1314.5	3147.7	0.8918	0.0013	0.11556	0.5368

VII. Mesh independence and validation

This section first deals with the solution independence of the network. In general, the solution independence from the grid means that by decreasing the stacking elements and in other words increasing the number of elements the resulting numerical result will not change much. So that the rate of change result is negligible compared to the increase in computational costs. A spiral tube with a circular cross-section is intended for this purpose. The pure water operating fluid is assumed and the fluid velocity at the inlet is assumed to be one meter per second. The heat flux on the pipe wall is also assumed to be 80 kW / m ^{2}. The average Nusselt number for the spiral tube is considered as a measure of the independence of the solution from the network. For this purpose, the average Nusselt number is calculated for three different shapes and is given in Table (3).

Table 3. Investigate solving independence from the medh

No	Number of element	Number of node	Average Nusselt number	Error percentage	Percentage of element number changes
1	754125	235480	232.45	%3.1	%21
2	954875	305414	239.87	%0.8	%14.6
3	1118694	353790	241.91		

As shown in Table 3, the average Nusselt number increased from 232.45 to 239.87 as the number of elements increased from 754125 to 954875, which represents a 21% increase in the number of elements, indicating a 3.1% change in the number Nusselt is average which is a lot. But with the increase in the number of elements from 954875 to 1118694, which represents a 14.6% increase in the number of elements, the average Nusselt number increased from 239.87 to 241.91, indicating a change of 0.8%, which is insignificant. So it can be said that the solution is network-independent.

For the validation of the numerical model developed in the present study, the numerical results are compared with the numerical data presented by Sunny et al[28]. They considered the pipe diameter 15.8 mm

and the operating fluid as water. The average Nusselt number calculated by Sunny et al [28] as well as the average Nusselt number calculated in the present study are compared in Fig. (2) for different values of inlet fluid mass flow rates.

As can be seen in Figure (2), the numerical data obtained from the model developed in the present study are in good agreement with the data presented by Mohaski and Parik [28], which represent the accuracy and precision of the model. Developed in the present study. The validated model can now be easily used to investigate the research parameters.

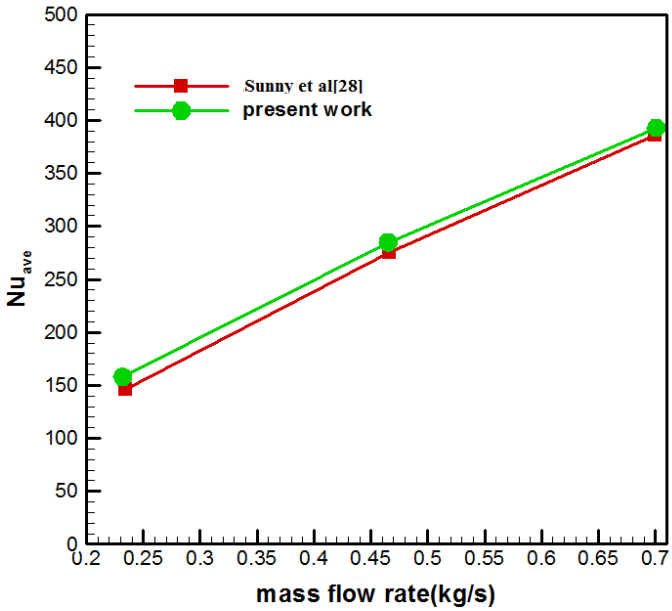

Figure 2. Comparison of numerical data of the present study with data presented by Mohaski and Parik [28]

VIII. Results

In this section, the average Nusselt number, local Nusselt number in three levels at 20, 30 and 40 cm heights, vorticityin the three levels, temperature in the three levels, heat transferred in the three levels, average friction coefficient and coefficient of friction The three levels will be calculated and reported for different amounts of nanofluid volume fraction and three input speeds of 0.5, 0.7 and 1 m / s. The calculations are first done for the spiral tube with a circular cross-section, then a square and then an elliptical.

Figure 3 shows the variations of the mean Nusselt number for different values of Reynolds number and different volume fraction in the spiral tube with circular cross-section.

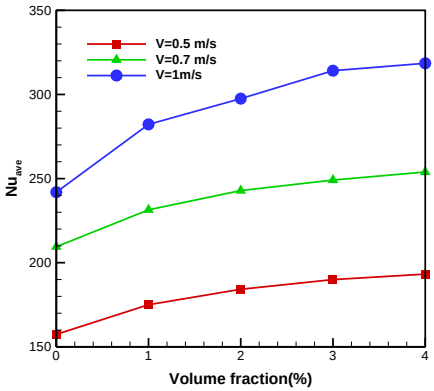

Figure 3. Changes in the mean Nusselt number for different values of Reynolds number and different volume fraction in spiral tube with circular cross section

Figure 4 shows the variations of the local Nusselt number for the inlet velocity of 1 m / s and the different volume fraction in the spiral tube with a circular cross-section at different heights.

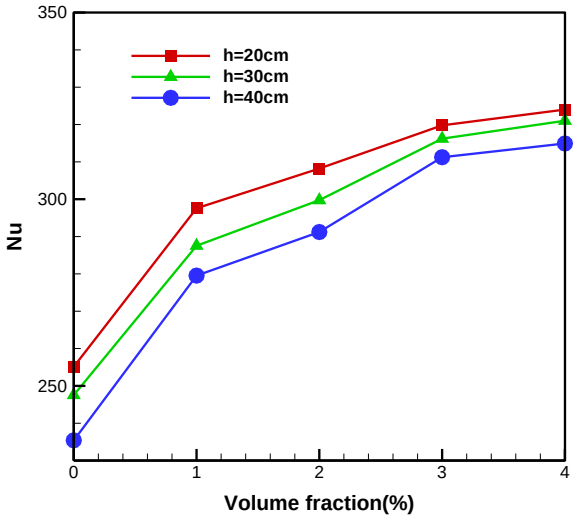

Figure 4. Local Nusselt number variations for 1 m / s inlet velocity and different volume fraction in spiral tube with circular cross section

Figures (5) and (6) can be seen to understand why the rate of heat transfer decreases with increasing altitude and how the increase in bulk temperature leads to a decrease in the temperature gradient and thus the local Nusselt number.

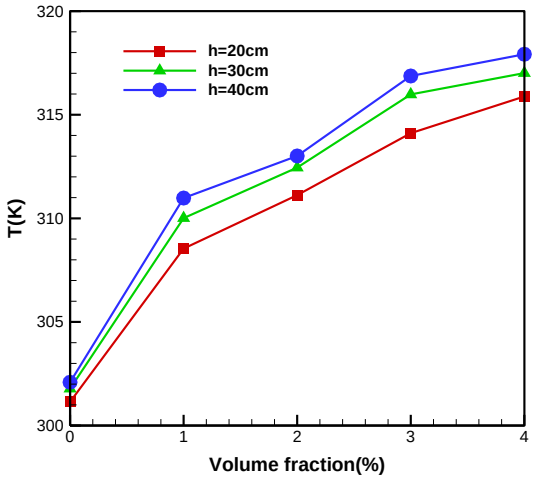

Figure 5. Variations of local bulb temperature for 1m / s inlet velocity and different volume fraction in spiral tube with circular cross section at different heights

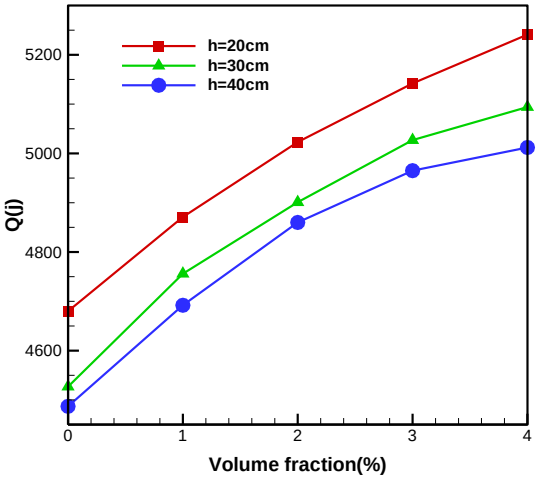

Figure 6. Localized heat transfer variations (in kilojoules) for one m / s inlet velocity and different volume fraction in spiral tube with circular cross section at different heights

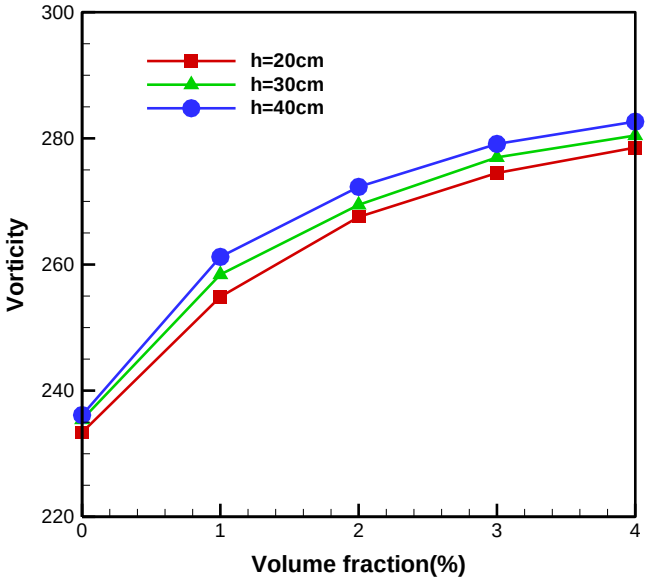

Figure 7. *Local Verticality Variations for Input Speeds of 1 m / s and Different Volume Fractions in a Spiral Pipe with Circular Cross-Section at Different Heights*

Figures (8) to (13) illustrate the diagrams of the above parameters for a spiral tube with a square cross-section.

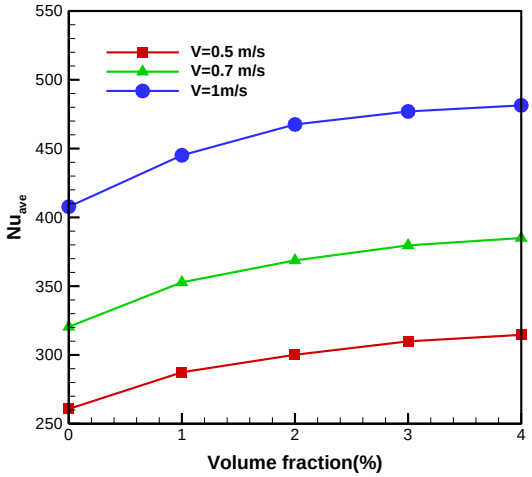

Figure 8. Modifications of the average Nusselt number for different values of Reynolds number and different volume fraction in a spiral tube with square cross section

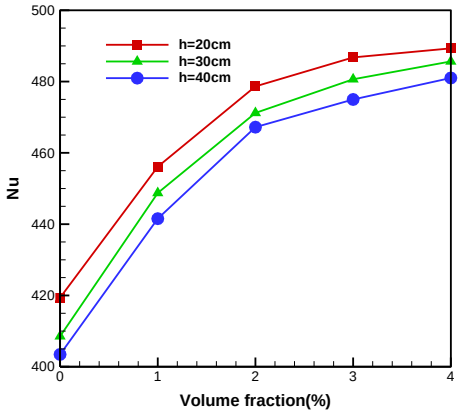

Figure 9. Variations of local Nusselt number for 1 m / s inlet velocity and different volume fraction in spiral tube with square cross section at different heights

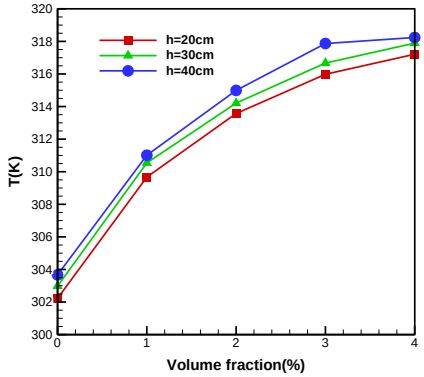

Figure 10. Localized block temperature variations for 1 m / s inlet velocity and different volume fraction in spiral tube with square cross section at different heights

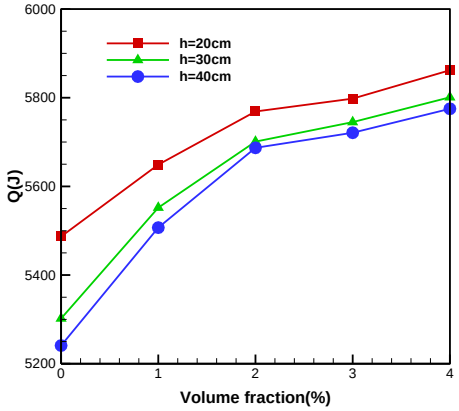

Figure 11. Localized heat transfer variations for 1 m / s inlet velocity and different volume fraction in spiral tube with square cross section at different heights

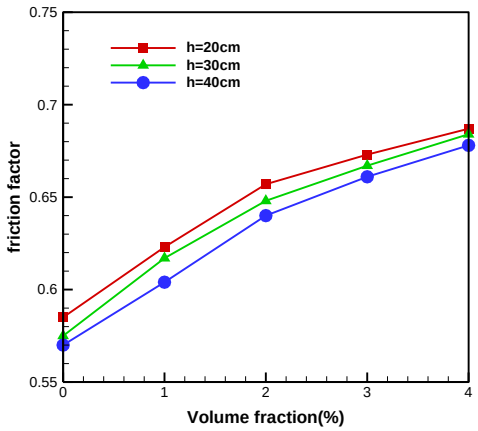

Figure 12. Variations of local friction coefficient for one meter / s inlet velocity and different volume fraction in spiral tube with square cross section at elevations

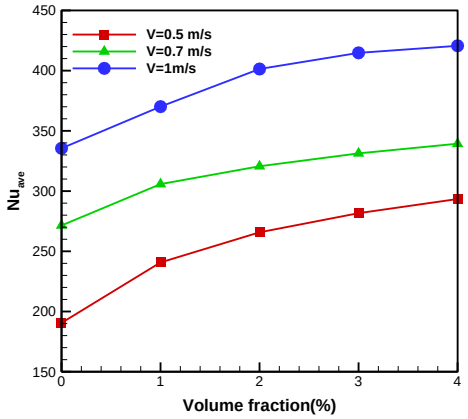

Figure 13. Variations of mean Nusselt number for different values of Reynolds number and different volume fraction in spiral tube with elliptic cross section

*Diagrams for a spiral tube with an elliptical cross-section are also shown in Figures (*14*) to (*19*)..*

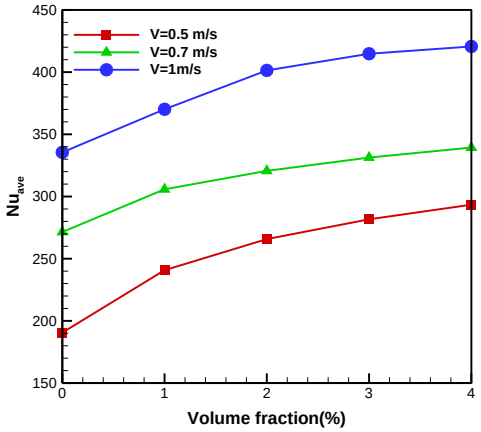

Figure 14. Variations of mean Nusselt number for different values of Reynolds number and different volume fraction in spiral tube with elliptic cross section

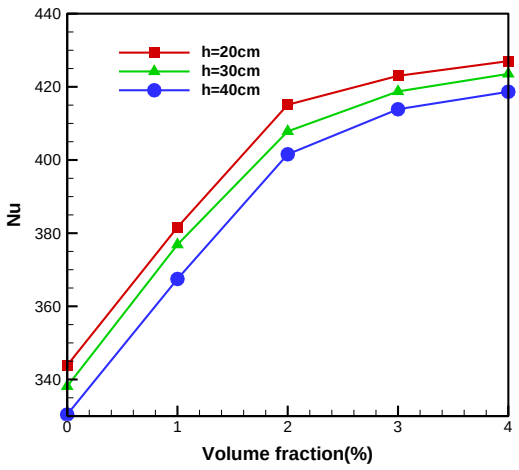

Figure 15. Variations of local Nusselt number for 1 m / s inlet velocity and different volume fraction in spiral tube with elliptic cross section at different heights

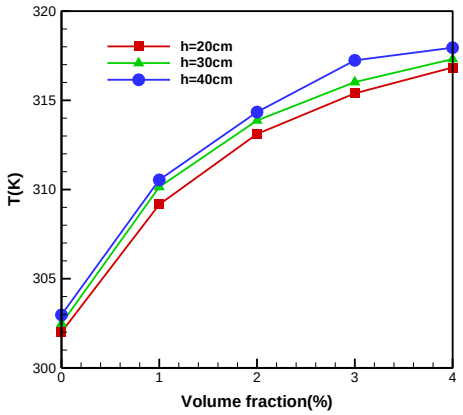

Figure 16. Variations of local ballast temperature for 1m / s inlet velocity and different volume fraction in spiral tube with elliptic cross section at different heights

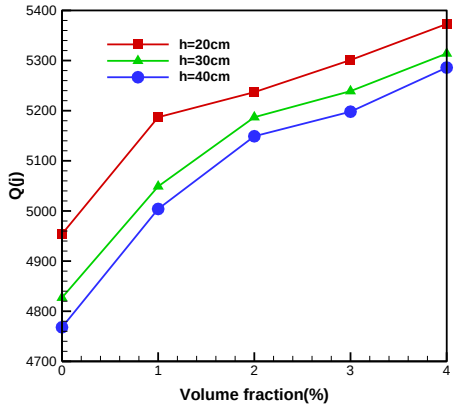

Figure 17. Topical heat transfer variations for 1 m / s inlet velocity and different volume fraction in spiral tube with elliptic cross section at different heights

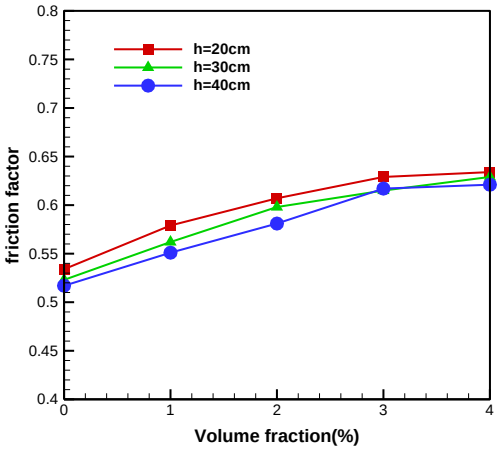

Figure 18. Variations of local friction coefficient for one meter / s inlet velocity and different volume fraction in spiral tube with elliptic cross section at different heights

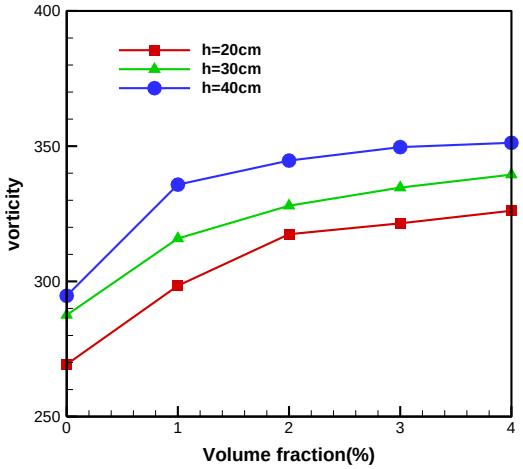

Figure 19. Local Verticality Variations for Input Speeds of 1 m/s and Different Volume Fractions in a Spiral Tube with an Elliptical Cross Surface at Different Heights

Finally in Figures (20) to (23) the variations of mean Nusselt number, local Nusselt number, coefficient of friction and vorticityare given for all three geometries.

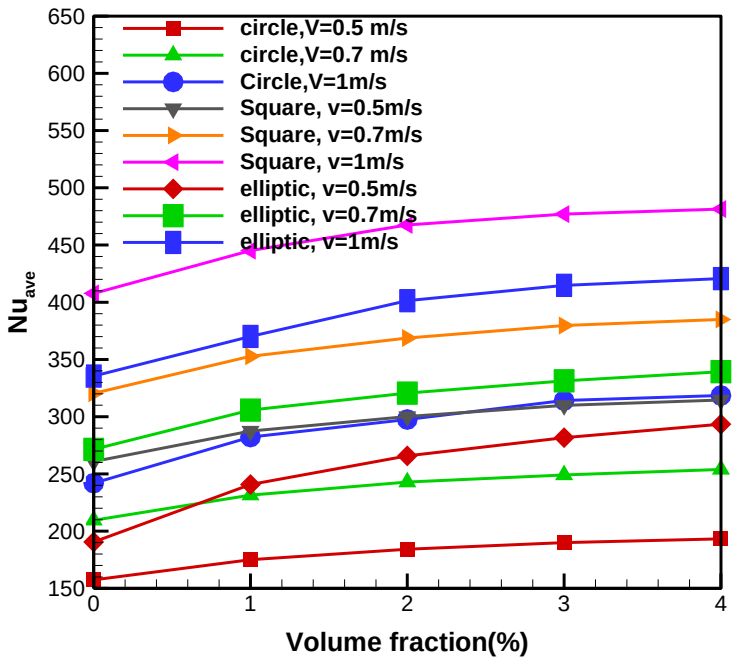

Figure 20. Comparison of the average Nusselt number for a spiral tube with three different cross sections

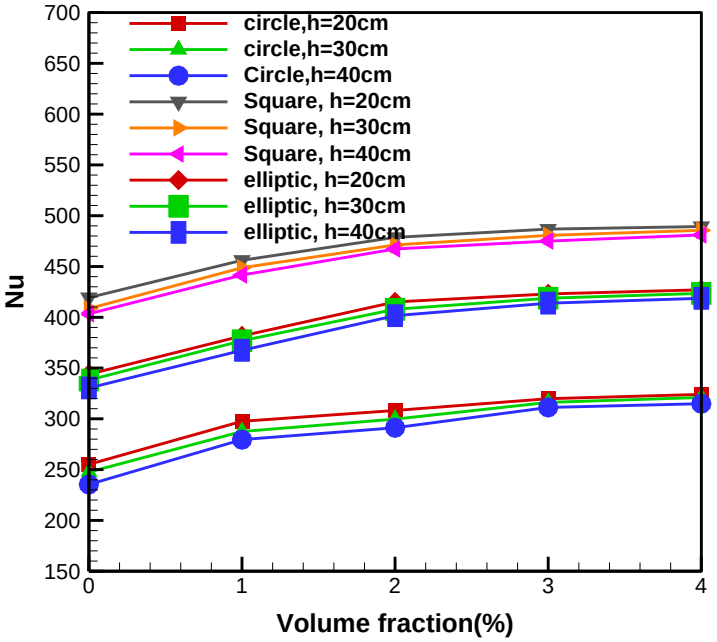

Figure 21. Comparison of local Nusselt number for spiral tube with three different cross sections at different heights

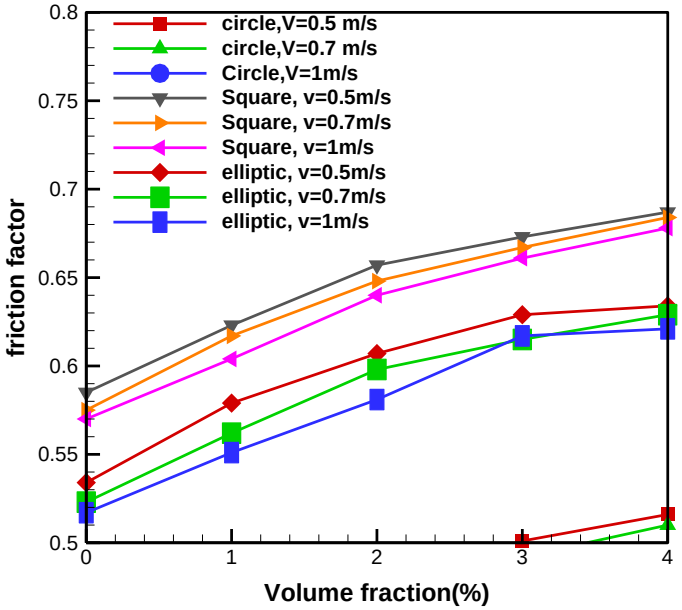

Figure 22. Comparison of the local coefficient of friction for a spiral tube with three different cross sections at different heights

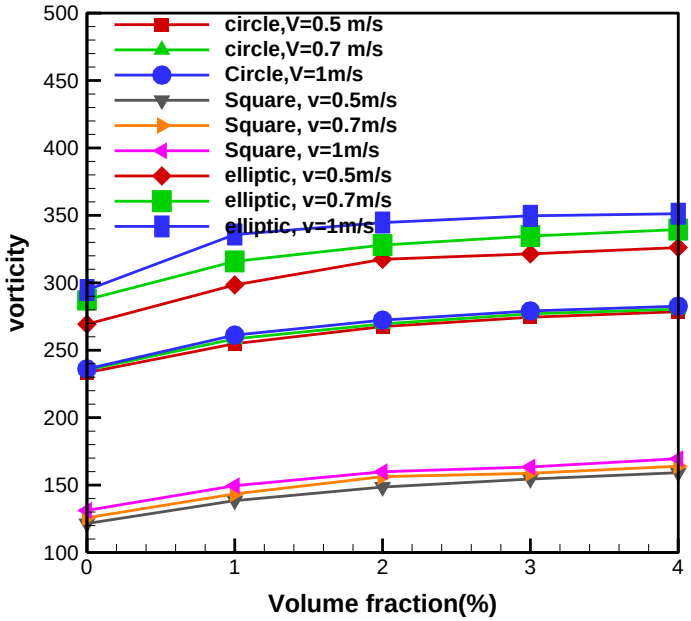

Figure 23. Comparison of local vorticity for spiral tube with three different cross sections at different heights

IX. Summary and Conclusion

It was shown that with increasing volume fraction and also with increasing fluid velocity (Reynolds number) the average Nusselt number increased. The average of the volume fraction is 3% to 4%. In other words, by increasing the volume fraction, a species saturation is created so that a further increase in the volume fraction has less effect on increasing the average Nusselt number. It should be noted that by increasing the volume fraction from 3% to 4% the agglomeration process may occur, which greatly reduces the average Nusselt number and thermal properties of the nanofluid. In general, increasing Reynolds number (turbulence flow) in the range of Reynolds numbers studied has a greater effect on increasing the average Nusselt number than adding nanoparticles. So for fluid inlet velocity of 0.5 m / s (Reynolds number about 2400) by adding nanoparticles to a volume fraction of 4% still the average Nusselt number is much lower than pure water fluid with Reynolds number about 5000. In other words, it can be concluded that although the use of nanoparticles in the base fluid improves the thermal properties of the fluid and thereby increases the rate of heat transfer, the effect of turbulent flow is still greater.

As the height increases, the Nusselt number decreases but the slope decreases. In other words, by increasing the height from 20 cm to 30 cm, the Nusselt number decreases by about 12 units, but by increasing the height from 30 cm to 40 cm, the Nusselt number decreases by about 18 units. Be it. This is because with increasing altitude as the heat flux transferred to the fluid increases and therefore the average fluid temperature increases, the rate of heat transfer, which is a function of the temperature gradient, decreases. In this case, as the volume fraction of nanosized particles increases, the average Nusselt number increases, especially at low volume fractions. With increasing altitude as the fluid is exposed to more heat flux, the temperature increases, resulting in an increase in fluid temperature. As the bulk temperature increases, the heat transfer potential between the pipe wall and the fluid decreases as the temperature gradient decreases. As the temperature rises due to the decrease in temperature gradient, the heat transfer rate decreases, resulting in the Nusselt number, which is a function of the heat transfer rate. As can be seen, the effect of using nanofluid on the heat transfer rate at 20 cm height is much greater than at 30 and 40 cm height. Also the height of 30 cm is approximately equal to the middle height of the spiral tube, which is the average Nusselt number at this height is almost equal to the average Nusselt number with a slight difference. As the height increases, the amount of vorticity increases. The reason for this can be found in the more confusing flow. This seems obvious given the spiral tube geometry that causes the vortex to form vorticity due to centrifugal forces entering the fluid. As the volume fraction of nanoparticles increases in the base fluid, the vorticity also increases. This is because with increasing density and the presence of particles in the fluid, the effect of centrifugal forces is better seen. It has also been shown that a spiral tube with a square cross-section generally exhibits the best thermal performance, followed by a spiral tube with an elliptical cross-section. In general, the spiral tube with a circular cross-section shows the weakest thermal performance among the three cross-sections examined. This equation can be found in the hydraulic diameter of the cross-section so that the hydraulic diameter of the square cross-section is obtained by 4, while the hydraulic diameter of the circular cross-section is 2. Thus the hydraulic diameter of the square cross-section is approximately twice that of the circular cross-section. For example, for a spiral tube with a

circular cross-section and a volume fraction of 4% the average Nusselt number is approximately equal to the average Nusselt number for a spiral tube with a square cross-section and a volume fraction of 4% and an input rate of 0.5 m / s.

In general, based on the comparative diagrams presented, it can be concluded that the spiral tube with square cross-section performs better. The average Nusselt number for a spiral tube with a square cross-section is about twice that of a circular cross-section.

Amir haghighatkhah, et. al. "Numerical Investigation of Non-Newtonian Nanofluid Flow in Spiral Pipe." *IOSR Journal of Mechanical and Civil Engineering (IOSR-JMCE)*, 17(6), 2020, pp. 22-37.